The Impact of Land Use and Land Cover Changes on Carbon Storage and Sequestration in Coastal Ecosystems and Along the Elevation Using InVEST Model and Google Earth Engine Platform

Songsom, V.,[1] Puangkaew, N.[2] and Kulsoontornrat, J.[3*]
[1]Faculty of Technology and Environment, Prince of Songkla University, Phuket Campus, Phuket 83120, Thailand
[2]Department of Geography, Faculty of Humanities and Social Sciences, Prince of Songkla University, Pattani Campus, Pattani 94000, Thailand
[3]Department of Geographic Information Science, School of Information and Communication Technology, University of Phayao, Muang Phayao 56000, Thailand
**Corresponding Author*

DOI: https://doi.org/10.52939/ijg.v22i3.4871

Abstract
Coastal ecosystems play a pivotal role in climate change mitigation through carbon storage and sequestration, yet they are increasingly threatened by land use and land cover (LULC) change. This study investigates the spatiotemporal impacts of LULC change on carbon dynamics in Phang Nga Bay, southern Thailand, from 2000 to 2020, with a focus on elevation gradients. By integrating the Random Forest algorithm in Google Earth Engine (GEE) with the Integrated Valuation of Ecosystem Services and Tradeoffs (InVEST) model, this study establishes a scalable, high-accuracy framework that overcomes the limitations of resource-intensive field assessments in complex coastal terrains. The results reveal extensive LULC changes, driven primarily by the expansion of oil palm plantations replacing evergreen and para rubber forests. These transitions led to a net carbon storage loss of approximately 821,000 Mg C, with the greatest losses occurring between 2000 and 2010. In contrast, mangrove forests, although covering only about one-fifth of the area, consistently contributed over 50 percent of carbon storage and showed localized gains in sequestration that offset some conversion losses. Carbon storage declined across all elevation zones, especially between 100 and 400 m, indicating agricultural expansion into upland forested areas. These findings highlight the need for elevation-sensitive land management and targeted conservation strategies that prioritize high-carbon ecosystems, particularly evergreen and mangrove forests, to ensure long-term carbon sequestration and resilience in tropical coastal landscapes.

Keywords: Carbon Storage and Sequestration, LULC Change, Coastal Ecosystems, Elevation, InVEST Model

1. Introduction

Coastal ecosystems, including mangroves, salt marshes, swamp forests, wetlands, and seagrass beds, provide long-term ecological and economic benefits. These ecosystems support vital services such as fisheries, aquaculture (e.g., shrimp farming), and tourism, and serve as biodiversity hotspots that contribute substantially to local and national economies. The economic value of these ecosystems has been estimated at approximately USD 190,000 per hectare in Indonesia and around 300 million Baht annually in Thailand [1] and [2]. In addition to their economic significance, coastal ecosystems play a key role in climate change mitigation by acting as natural carbon sinks that capture and store atmospheric carbon dioxide [3][4] and [5]. Estimates from the United Kingdom suggest that preserving existing coastal habitats could yield approximately £1 billion in carbon sequestration benefits between 2000 and 2060, while continued habitat loss could reduce this capacity by £0.25 billion, assuming a 3.5 percent discount rate [6]. Land use and land cover (LULC) changes significantly influence both biodiversity and carbon storage potential. These changes contribute to ecological degradation and elevate greenhouse gas emissions, thereby exacerbating climate change [7] and [8].

In coastal areas, the effects of LULC change are particularly complex, as land conversion not only spreads horizontally but also follows elevation gradients [9][10] and [11]. Despite this, limited research has examined the interactions between elevation-specific land cover changes and their implications for carbon sequestration. Understanding this spatially explicit relationship is crucial for effective land management, zoning regulations, and climate resilience planning, especially in vulnerable coastal zones.

Although field-based carbon assessments offer high accuracy across various ecosystems such as mangroves, oil palm plantations, and evergreen forests [12][13][14] and [15], such methods are often resource-intensive and less feasible for large or topographically diverse areas. Modelling approaches such as the Integrated Valuation of Ecosystem Services and Tradeoffs (InVEST) offer practical alternatives by enabling spatially explicit quantification and visualization of ecosystem services based on land cover inputs [16][17] and [18]. The InVEST model has been successfully applied in a wide range of environments, including arid, urban, mountainous, and agricultural systems [19][20][21] and [22], and is increasingly used to evaluate carbon storage dynamics in coastal areas [23][24] and [25].

The recent development of cloud-based geospatial platforms, particularly Google Earth Engine (GEE), has further enhanced the capacity to analyze LULC dynamics. GEE provides access to multi-temporal satellite imagery and analytical tools within a scalable infrastructure, enabling efficient land cover classification and elevation-based spatial analyses [19]. This study integrates the InVEST carbon storage and sequestration model with the GEE platform to assess the spatiotemporal impacts of LULC changes on both carbon storage and sequestration in Phang Nga Bay, southern Thailand, from 2000 to 2020. Particular attention is given to the elevation dimension of these changes, providing insights into how land cover transitions at different altitudes affect regional carbon dynamics. The results contribute to a better understanding of elevation-sensitive land transformation and inform sustainable land use planning and conservation strategies in tropical coastal ecosystems.

2. Materials and Methods

2.1 Study Area

Phang Nga Bay, located in southern Thailand (Figure 1), is a shallow coastal bay renowned for its scenic limestone islands, sandy beaches, and biodiversity-rich ecosystems. Geologically, the bay features sedimentary and metamorphic rock formations with widespread limestone outcrops, leading to karst landforms such as caves and sinkholes. Coastal subsidence has shaped its rugged coastline, forming numerous inlets and islands.

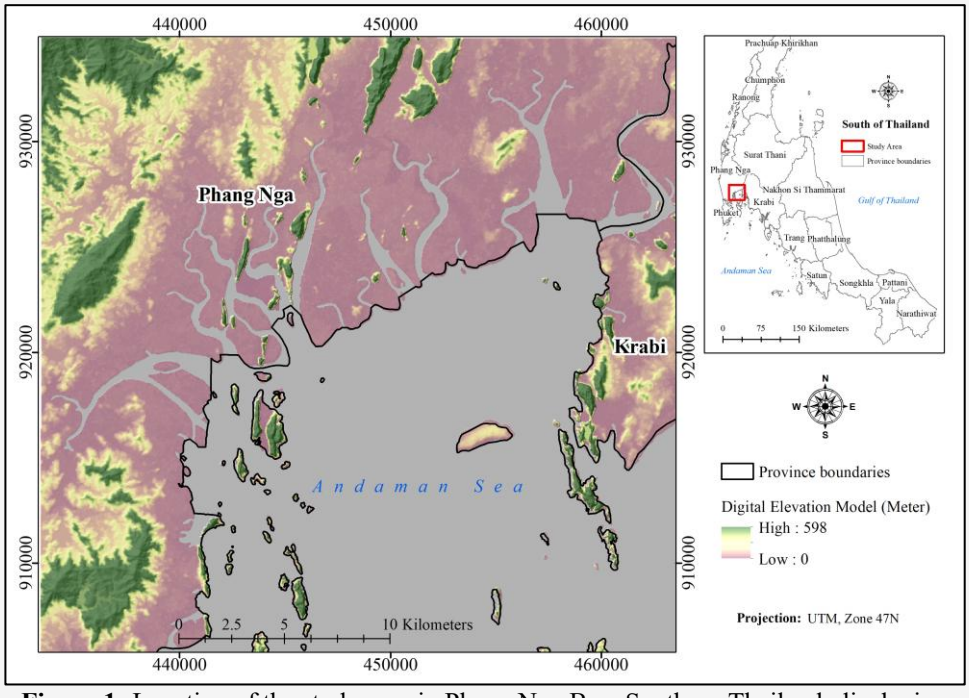

Figure 1: Location of the study area in Phang Nga Bay, Southern Thailand, displaying the Digital Elevation Model (DEM) and provincial boundaries

The region has a tropical monsoon climate with two seasons: a dry season (November–April) and a rainy season (May–October), receiving an average annual rainfall of approximately 2,300 millimeters. Ecologically, the bay includes mangrove forests, coral reefs, and seagrass beds, which support diverse marine life. Protected areas such as Ao Phang Nga National Park (Established in 1981) and its designation as a Ramsar Site in 2002 highlight its ecological significance. However, the area is increasingly threatened by tourism development and resource exploitation, posing risks to its environmental integrity [26][27] and [28].

2.2 Methods

The methodology for this study comprises the following steps: data collection and preparation, LULC classification and change detection, carbon storage and sequestration estimation using the InVEST model, and calculation of changes in carbon storage for each LULC type along elevation, as illustrated in the flowchart (Figure 2).

2.2.1 Data collection and preparation

Landsat imagery from the Landsat 5 and Landsat 8 Collection 2 Level-2 Surface Reflectance (SR) datasets was obtained via GEE to assess LULC changes in Phang Nga Bay for the years 2000, 2010, and 2020. These SR products include standardized atmospheric correction performed by the USGS, with Landsat 5 processed using the Landsat Ecosystem Disturbance Adaptive Processing System (LEDAPS) and Landsat 8 using the Land Surface Reflectance Code (LaSRC), ensuring radiometric consistency across sensors and eliminating the need for additional atmospheric correction. All Collection 2 Level-2 datasets also incorporate precision terrain correction and sensor-level geometric alignment using consistent ground control points and DEM-based adjustments, providing sub-pixel co-registration across acquisition years and minimizing misalignment-induced change artifacts.

For each reference year (2000, 2010, and 2020), all Landsat scenes covering the study area and acquired between 1 January and 31 December with less than 15% cloud cover were selected. These scenes were refined using per-pixel QA information from the QA_PIXEL band. Cloud and shadow masking was performed by excluding pixels labeled as clouds or cloud shadows under the CFMask algorithm, ensuring consistent and robust atmospheric screening across all three years. After masking, sensor-specific scale factors were applied to the optical SR bands to convert digital numbers to surface reflectance values. The remaining high-quality images were then combined into an annual multi-scene median mosaic composite for each year, which helped smooth residual haze, illumination differences, and intra-annual variability. Each mosaic was subsequently clipped to the Phang Nga Bay boundary using a region of interest (ROI) imported from ArcGIS. The final feature stack for classification comprised all Landsat spectral bands, key spectral indices (NDVI, MNDWI, NDBI, NSDSI3, SAVI, EVI, and MBI; see Appendix A: Table A1), and Shuttle Radar Topography Mission (SRTM) elevation data, providing a robust and informative dataset for Random Forest–based LULC classification.

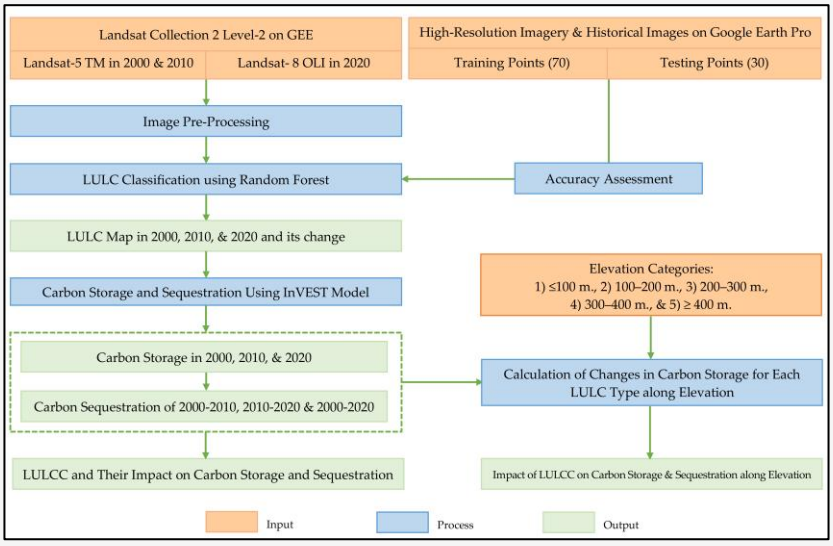

Figure 2: Methodological workflow integrating Random Forest classification, InVEST carbon modeling, and assessment of carbon dynamics along elevation gradients

2.2.2 Land Use and Land Cover classification and change detection

LULC classification for Phang Nga Bay was carried out using the Random Forest (RF) algorithm on the GEE platform. Seven major LULC categories were defined based on current land use patterns and observed landscape characteristics. These categories include Urban and built-up area (Ur), Oil palm (Op), Para rubber (Pr), Evergreen forest (Ef), Mangrove forest (Mf), Waterbody (Wa), and Bare land (Bl).

For each target year (2000, 2010, and 2020), reference samples were collected through visual interpretation of high-resolution historical imagery in Google Earth Pro. A class-wise stratified random sampling approach was applied to ensure adequate representation of all LULC categories, utilizing stratification by land-cover class rather than proportional area to mitigate the under-representation of minority classes. The samples were subsequently partitioned into two independent subsets: 70% used for training the RF model and 30% reserved exclusively for accuracy assessment. The RF algorithm was selected for its robust performance in high-dimensional data environments, resistance to overfitting, and interpretability. The algorithm operates by generating an ensemble of decision trees, each trained on a random data subset, and aggregates predictions via majority voting [29]. This methodology enhances both model generalization and classification accuracy [30] and [31].

The classification accuracy was evaluated using a confusion matrix generated from the validation samples within GEE. Two commonly used performance metrics were applied: overall accuracy (OA) and the Kappa coefficient (K). Overall accuracy represents the percentage of correctly classified validation samples, while the Kappa coefficient measures the agreement between predicted and actual classifications after accounting for chance agreement [32] and [33]. Both metrics were computed using the ee.Classifier.confusionMatrix() function, providing a consistent evaluation of model performance.

Following classification, LULC changes were analyzed using a post-classification comparison technique. This method detects transitions between land cover types by comparing classified maps from different years. Change detection was conducted for three-time intervals: 2000 to 2010, 2010 to 2020, and 2000 to 2020. This approach enabled the identification of specific "from-to" land cover conversions and provided a comprehensive understanding of spatiotemporal dynamics within the Phang Nga Bay area [34].

2.2.3 Carbon storage estimation using the InVEST model

The InVEST model has been widely utilized to assess carbon storage, an essential ecosystem service [35][36][37][38][39] and [40]. The carbon storage module categorizes ecosystem carbon storage into four fundamental carbon pools: aboveground biological carbon (in all living plant biomass above the soil), belowground biological carbon (in the living root systems), soil organic carbon (distributed in organic and mineral soils), and dead organic carbon (in litter and dead trees) [41]. The module employs a simplified carbon cycle approach, utilizing each LULC type as the assessment unit. It calculates the carbon density and storage for each grid cell based on its respective LULC type, thereby estimating both carbon storage and sequestration potential [19] and [42]. For this study, various carbon pool parameters were obtained by reviewing different literature sources based on the LULC classification (Table 1). These parameters were then incorporated into Equations 1 [43] and [44], and Equations 2 [45] to calculate the total carbon storage (C) and carbon sequestration (S) for the study area. Although the units of carbon pools in the reference are expressed per hectare (ha), this study presents the values per square kilometer (km^2).

$$C = \sum_{k=1}^{n} A_k \times (C_{k,a} + C_{k,b} + C_{k,s} + C_{k,d}) \quad \text{Equation 1}$$

Where C is the total carbon storage in the study area, A_k is the area of LULC type k, and the four parameters of carbon density in LULC type k are above-ground biomass ($C_{k,a}$, Mg C ha^{-1}), belowground biomass ($C_{k,b}$, Mg C ha^{-1}), soil organic carbon ($C_{k,s}$, Mg C ha^{-1}), and dead organic matter ($C_{k,d}$, Mg C ha^{-1}).

$$S = C^{T2} - C^{T1} \quad \text{Equation 2}$$

Where C^{T2} and C^{T1} denote the total carbon storage in the future year ($T2$) and current year ($T1$), respectively.

2.2.4 Carbon storage change along elevation

To analyze the effects of LULC change on carbon storage along elevation gradients, the study area was stratified into five elevation levels: (1) lower than 100 meters, (2) 100–200 meters, (3) 200–300 meters, (4) 300–400 meters, and (5) more than 400 meters above mean sea level. For each elevation level, total carbon storage was calculated for the years 2000, 2010, and 2020 using outputs from the InVEST Carbon Storage and Sequestration model.

Table 1: Carbon pools (Mg C ha^{-1}) for different LULC types

LULC types	Above-Ground Organisms	Underground Organisms	Soil	Dead Organic Matter	References
Urban and built-up area	0.00	0.00	0.00	0.00	[18] and [46]
Oil palm	73.76[a]	16.00[b]	55.80[c]	3.68[d]	[a] [47] [b] [48] [c] [49] [d] [50]
Para rubber	50.73	11.91	113.45	3.55	[22]
Evergreen forest	112.50	32.70	238.00	43.40	[35]
Mangrove forest	67.95	29.85	341.33	3.90	[51]
Waterbody	0.16	0.00	3.29	3.29	[52]
Bare land	0.10	0.00	9.60	0.00	[20]

Table 2: Accuracy assessment of LULC

Class	2000				2010				2020			
	PA	UA	OA (%)	K	PA	UA	OA (%)	K	PA	UA	OA (%)	K
Ur	0.79	1.00			1.00	0.96			1.00	1.00		
Op	0.94	0.98			0.97	0.97			0.98	0.96		
Pr	0.98	0.92			0.98	0.97			0.97	0.97		
Ef	0.94	0.98	95.38	0.94	0.95	0.98	97.59	0.97	0.95	0.98	97.19	0.97
Mf	0.99	1.00			1.00	1.00			0.99	1.00		
Wa	0.96	1.00			0.98	0.98			0.94	0.96		
Bl	0.97	0.90			0.94	0.91			0.95	0.93		

To assess temporal dynamics, trend analysis was conducted to estimate the rate of change in carbon storage at each elevation level. In addition, the contribution of each LULC transition to carbon storage change within each elevation zone was quantified. The LULC classification consisted of seven categories, yielding a total of 42 transition classes. Only pixels with changes in land use between time periods were considered in the analysis. This approach follows similar methodologies applied in elevation-based LULC change studies, such as that of [10], which demonstrated the effectiveness of elevation-stratified analysis for understanding vegetation and carbon dynamics.

3. Results and Discussion

3.1 LULC Assessment and Change in Phang Nga Bay Using RF and GEE

The RF classification performed on the GEE platform produced consistently high-accuracy LULC maps for 2000, 2010, and 2020, with overall accuracies exceeding 95% and Kappa coefficients above 0.94 (Table 2). The strong class-wise Producer's and User's Accuracies further confirm the reliability of the classification across all land cover categories. These results are consistent with previous applications of GEE for multi-temporal land-cover analysis in coastal and wetland environments, which similarly demonstrate the platform's robustness and the strong performance of machine-learning classifiers such as RF in complex landscapes [53][54] and [55]. The inclusion of spectral indices (e.g., NDVI, MNDWI, NDBI) enhanced separability among vegetation- and water-related classes, while the 70–30 training–validation split and the use of visually interpreted reference samples provided a sound basis for model generalization. The scalability and computational capacity of GEE additionally facilitated efficient processing of the multi-decadal Landsat dataset [56].

Throughout the study period, waterbodies consistently remained the dominant land cover class (Table 3), followed by mangrove forests and para rubber plantations during 2000 and 2010. However, by 2020, the landscape underwent a significant shift due to the marked expansion of oil palm plantations, which increased to cover 16.62% of the total area. This expansion occurred largely at the expense of evergreen forest, para rubber, and bare land. Consequently, evergreen forest exhibited a continuous decline, dropping from 10.63% in 2000 to 5.55% in 2020. These changes, illustrated in Figure 3, indicate a clear pattern of deforestation and agricultural conversion within the study area over the two decades. The post-classification change detection identifies oil palm expansion as the primary driver of land transformation throughout the study period (Tables 4-5).

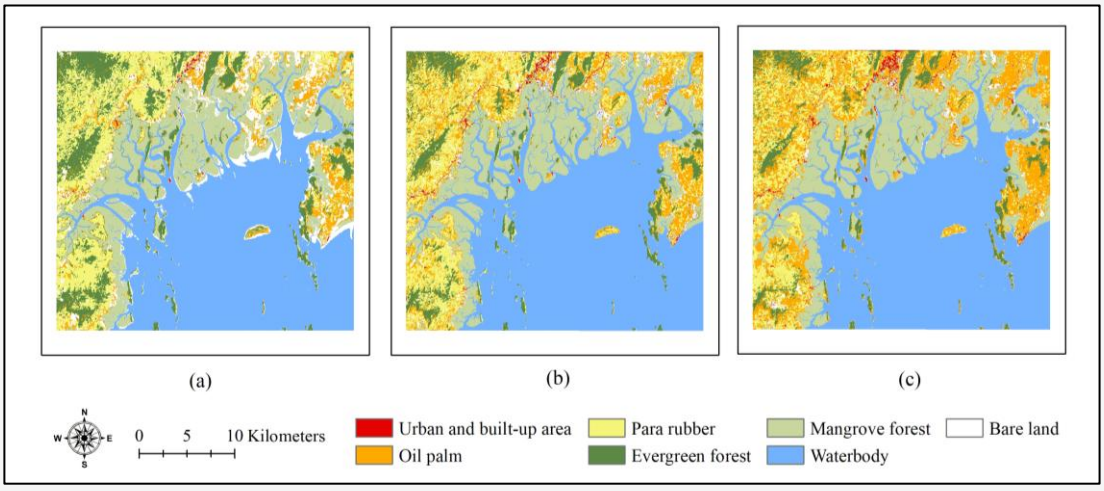

Figure 3: Spatial distribution of LULC classification in (a) 2000, (b) 2010, and (c) 2020

Table 3: Area and percentage of LULC data in 2000, 2010, and 2020

No	LULC type	LULC data in 2000		LULC data in 2010		LULC data in 2020	
		Area (km^2)	Percent	Area (km^2)	Percent	Area (km^2)	Percent
1	Urban and built-up area (Ur)	2.62	0.29	7.64	0.84	9.45	1.04
2	Oil palm (Op)	54.11	5.95	95.13	10.45	151.29	16.62
3	Para rubber (Pr)	129.24	14.20	128.19	14.08	98.90	10.87
4	Evergreen forest (Ef)	96.73	10.63	62.54	6.87	50.54	5.55
5	Mangrove forest (Mf)	175.64	19.30	176.58	19.40	182.00	20.00
6	Waterbody (Wa)	382.78	42.06	416.77	45.79	398.71	43.81
7	Bare land (Bl)	69.06	7.59	23.34	2.56	19.28	2.12
	Total	**910.18**	**100.00**	**910.18**	**100.00**	**910.18**	**100.00**

Table 4: Transitional matrix of LULC change between 2000 and 2010

	LULC types	LULC in 2010 (km^2)							
		Ur	Op	Pr	Ef	Mf	Wa	Bl	Total
LULC in 2000 (km^2)	Urban and built-up area (Ur)	1.95	0.04	0.33	0.01	0.00	0.03	0.25	**2.62**
	Oil palm (Op)	0.75	32.92	11.71	2.03	3.87	0.20	2.64	**54.11**
	Para rubber (Pr)	0.45	34.67	86.32	3.12	0.00	0.03	4.64	**129.24**
	Evergreen forest (Ef)	0.16	17.51	17.59	54.35	2.39	3.57	1.16	**96.73**
	Mangrove forest (Mf)	0.06	0.89	0.16	1.14	167.70	5.32	0.37	**175.64**
	Waterbody (Wa)	0.01	0.02	0.03	0.73	0.03	381.77	0.18	**382.78**
	Bare land (Bl)	4.26	9.09	12.04	1.14	2.58	25.85	14.10	**69.06**
	Total	**7.64**	**95.13**	**128.19**	**62.54**	**176.58**	**416.77**	**23.34**	**910.18**

Table 5: Transitional matrix of LULC change between 2010 and 2020

	LULC types	LULC in 2020 (km^2)							
		Ur	Op	Pr	Ef	Mf	Wa	Bl	Total
LULC in 2010 (km^2)	Urban and built-up area (Ur)	4.28	0.87	1.28	0.04	0.02	0.04	1.11	**7.64**
	Oil palm (Op)	0.76	67.23	22.33	2.64	0.87	0.04	1.27	**95.13**
	Para rubber (Pr)	1.88	56.45	63.89	2.42	0.13	0.06	3.38	**128.19**
	Evergreen forest (Ef)	0.05	13.59	5.47	41.58	1.44	0.19	0.22	**62.54**
	Mangrove forest (Mf)	0.03	5.19	0.05	0.79	170.20	0.12	0.20	**176.58**
	Waterbody (Wa)	0.20	0.95	0.25	2.77	9.00	397.41	6.18	**416.77**
	Bare land (Bl)	2.26	7.02	5.63	0.30	0.34	0.86	6.92	**23.34**
	Total	**9.45**	**151.29**	**98.90**	**50.54**	**182.00**	**398.71**	**19.28**	**910.18**

Table 6: Transitional matrix of LULC change between 2000 and 2020

LULC types		LULC in 2020 (km²)							
		Ur	Op	Pr	Ef	Mf	Wa	Bl	Total
LULC in 2000 (km²)	Urban and built-up area (Ur)	2.03	0.11	0.30	0.01	0.00	0.00	0.17	**2.62**
	Oil palm (Op)	1.26	39.37	8.42	0.73	2.68	0.09	1.57	**54.11**
	Para rubber (Pr)	1.42	57.55	65.54	1.90	0.01	0.01	2.80	**129.24**
	Evergreen forest (Ef)	0.13	31.72	15.41	44.23	3.29	1.04	0.91	**96.73**
	Mangrove forest (Mf)	0.05	3.65	0.10	1.13	169.76	0.63	0.33	**175.64**
	Waterbody (Wa)	0.02	0.10	0.05	1.33	0.84	378.02	2.42	**382.78**
	Bare land (Bl)	4.54	18.78	9.10	1.20	5.42	18.92	11.09	**69.06**
Total		**9.45**	**151.29**	**98.90**	**50.54**	**182.00**	**398.71**	**19.28**	**910.18**

This trend was characterized by the consistent replacement of para rubber and evergreen forest with oil palm plantations in both decades. Over the full twenty-year period, oil palm area expanded by approximately 97.16 km², predominantly through the conversion of para rubber (57.55 km²), evergreen forest (31.72 km²), and bare land (18.78 km²) (Table 6). These transitions align closely with national development initiatives, including the Palm Oil Industry Strategic Plan [57], government support policies [58], and rising global demand for biodiesel as a renewable energy source [59]. Additionally, bare land exhibited transient behavior throughout the study period, initially declining due to conversion into plantations but reappearing in certain locations following plantation clearing cycles. A noteworthy apparent conversion of bare land to waterbodies was also observed; however, visual interpretation of satellite imagery attributes this primarily to tidal variation. Specifically, the 2000 imagery captured low tide conditions that exposed sandy coastlines, whereas the 2020 imagery coincided with high tide conditions that inundated these areas. This finding highlights the critical importance of accounting for environmental dynamics when interpreting land cover changes in coastal zones.

Overall, the integration of RF and GEE proved effective for comprehensive monitoring of LULC dynamics in Phang Nga Bay. The observed patterns, characterized by agricultural expansion, forest decline, and environmentally driven coastal variability, reflect substantial landscape reorganization within the study area. The moderate spatial resolution and multi-decadal continuity of the Landsat archive enabled reliable detection of these changes. These results provide an essential foundation for subsequent analyses of carbon storage and sequestration, as the dominant LULC transitions identified here directly underpin the spatial–temporal carbon dynamics discussed in later sections.

3.2 Assessment of Carbon Storage and Sequestration Using the InVEST Model and the Impacts of Land Use and Land Cover Changes

In this study, the three decadal years (2000, 2010, and 2020) were selected to monitor long-term LULC changes, enabling the detection of major land transformation patterns and the associated shifts in carbon storage and sequestration. The results from the InVEST model indicate a significant decline in total carbon storage within Phang Nga Bay, decreasing from approximately 15,360,000 Mg C in 2000 to 14,540,000 Mg C in 2020, representing a net reduction of approximately 821,000 Mg C over the study period (Figure 4). The sharpest decline occurred between 2000 and 2010, driven primarily by the conversion of evergreen forests into para rubber and oil palm plantations. This transformation closely aligns with Thailand's strategic plan (2004–2029) aimed at promoting palm oil cultivation, and reflects broader land use trends observed across Southeast Asia, where the rapid expansion of oil palm has resulted in extensive deforestation and significant losses of carbon stocks [60] and [61]. Thailand's national policy appears to have played a catalytic role in accelerating such transformations, mirroring policy-driven deforestation patterns in countries like Indonesia and Malaysia [62].

The observed decline in carbon storage is strongly associated with the reduction of forested areas, particularly evergreen forests, which, along with mangrove forests, represent the two LULC types with the highest carbon pool values in the region. The replacement of these high-carbon ecosystems with land uses that have lower carbon storage potential, significantly undermines the landscape's capacity to sequester and retain carbon over time, thereby contributing to the net reduction in carbon storage observed throughout the two-decade period. An overview of carbon sequestration across different LULC types reveals notable differences in carbon dynamics during the study period (Table 7).

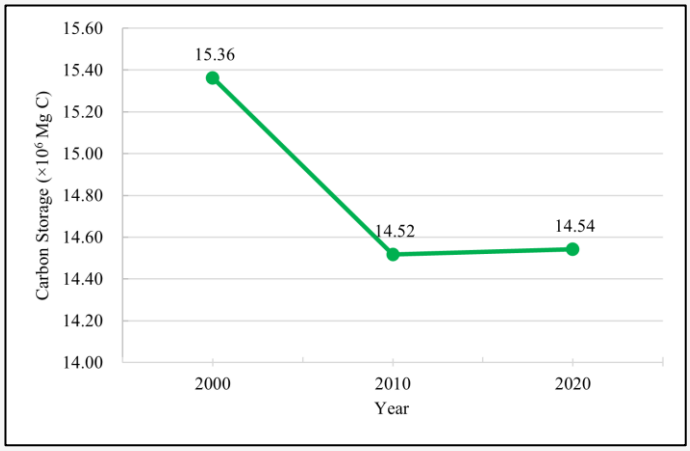

Figure 4: Total carbon storage in the years 2000, 2010, and 2020

Table 7: Carbon storage and sequestration across different LULC types between 2000 and 2020

LULC Type	Carbon storage (Mg C)						Carbon sequestration (Mg C)		
	2000	%	2010	%	2020	%	2000–2010	2010–2020	2000–2020
Urban and built-up area (Ur)	0.00	0.00	0.00	0.00	0.00	0.00	0.00	0.00	0.00
Oil palm (Op)	807,561.44	5.26	1,419,746.84	9.78	2,257,838.30	15.53	612,185.40	838,091.46	1,450,276.87
Para rubber (Pr)	2,321,732.12	15.11	2,302,880.70	15.86	1,776,722.30	12.22	−18,851.42	−526,158.39	−545,009.82
Evergreen forest (Ef)	4,126,702.00	26.86	2,667,845.29	18.38	2,156,091.70	14.83	−1,458,856.71	−511,753.59	−1,970,610.30
Mangrove forest (Mf)	7,781,157.35	50.65	7,822,824.33	53.89	8,063,137.09	55.45	41,666.97	240,312.76	281,979.73
Waterbody (Wa)	257,992.43	1.68	280,903.11	1.94	268,731.68	1.85	22,910.67	−12,171.43	10,739.25
Bare land (Bl)	66,987.04	0.44	22,635.14	0.16	18,705.77	0.13	−44,351.89	−3,929.37	−48,281.27
Total	**15,362,132.38**	**100.00**	**14,516,835.41**	**100.00**	**14,541,226.85**	**100.00**	**−845,296.98**	**24,391.44**	**−820,905.54**

Evergreen forests exhibited the largest net carbon loss (approximately 1,970,000 Mg C), whereas oil palm plantations demonstrated the highest sequestration gain (approximately 1,450,000 Mg C), a sharp increase driven directly by their expanded spatial footprint. Mangrove forests also contributed positively with a net gain of approximately 282,000 Mg C, demonstrating the resilience of these ecosystems. In contrast, para rubber plantations experienced a significant reduction of approximately 545,000 Mg C, indicative of both area decline and lower carbon density relative to the forests they replaced. Other land cover types showed only minor changes during the same period. Spatial analysis revealed substantial heterogeneity in the distribution of carbon storage across Phang Nga Bay, with the highest concentrations located in coastal zones and western upland areas predominantly covered by mangrove and evergreen forests (Figure 5). These ecosystems are recognized for their exceptional carbon sequestration potential, attributable to their dense aboveground biomass and substantial soil organic carbon stocks. The overall reduction in carbon storage over the two-decade period, averaging approximately 14,810,000 Mg C across the years 2000, 2010, and 2020, is closely associated with the spatial fragmentation and conversion of high-carbon land cover types.

Spatial changes in carbon sequestration over the study period further illustrate these dynamics (Figure 6). Between 2000 and 2010, notable reductions were observed primarily in coastal and hillside regions (Figure 6(a)), attributed to the rapid expansion of oil palm and para rubber plantations that replaced high-carbon evergreen forests. Coastal carbon storage was further impacted by tidal influences, as areas classified as bare land in 2000 were predominantly reclassified as water bodies by 2010, resulting in additional carbon losses. During the subsequent period from 2010 to 2020, spatial patterns of carbon storage change became more dispersed, although persistent declines occurred, especially in the southwestern hills (Figure 6(b)). These reductions were largely due to continued agricultural expansion, particularly for oil palm plantations. Overall, the long-term spatial analysis (Figure 6(c)) indicates a pattern of rapid initial forest conversion followed by slower, more fragmented land use changes, a trend consistent with deforestation dynamics observed in other tropical regions [63] and [64].

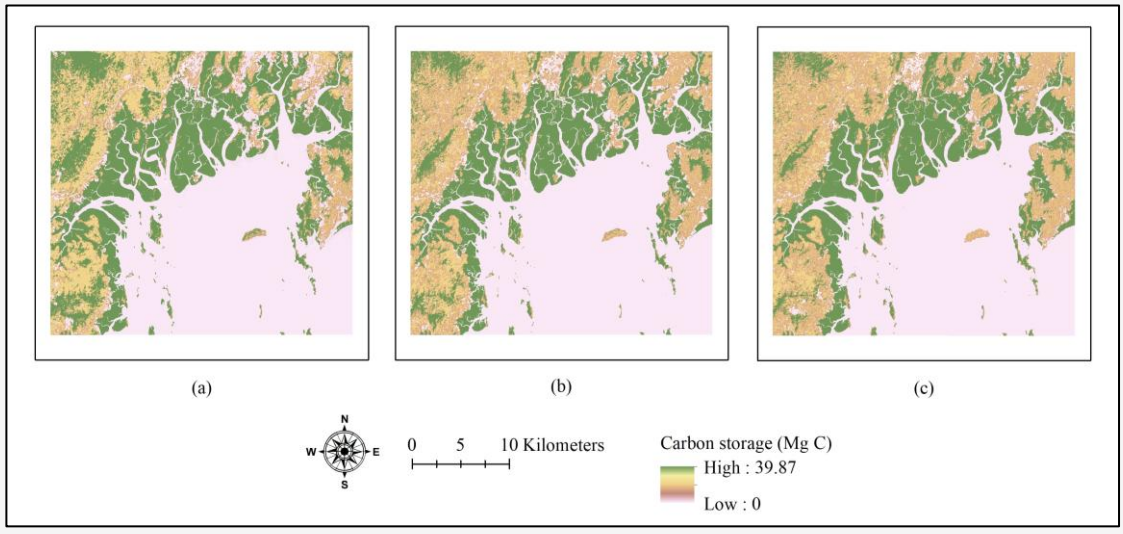

Figure 5: Spatial distribution of carbon storage in Phang Nga Bay in different years: (a) 2000, (b) 2010, and (c) 2020

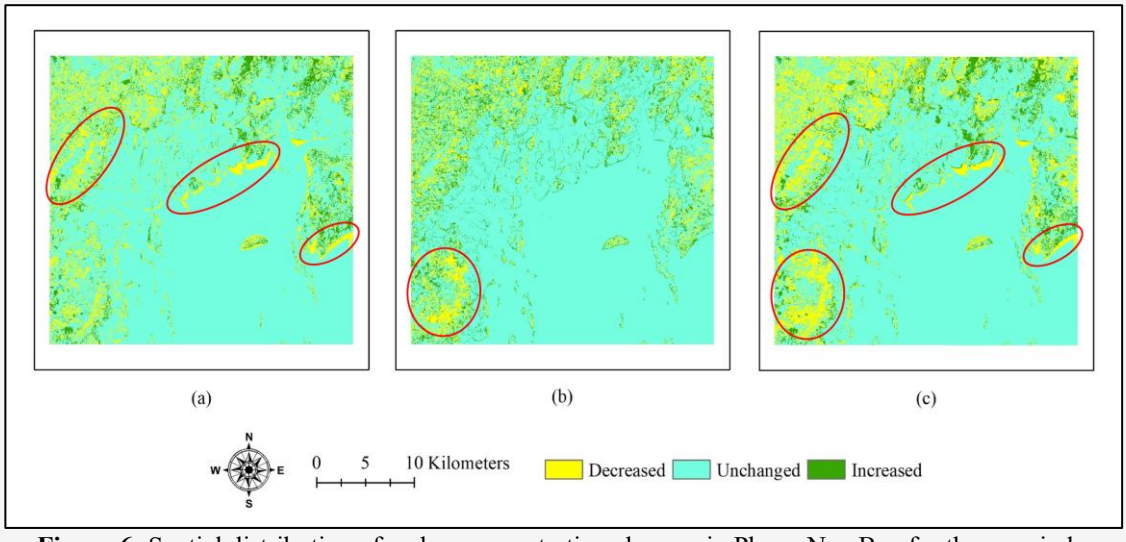

Figure 6: Spatial distribution of carbon sequestration changes in Phang Nga Bay for three periods: (a) 2000–2010, (b) 2010–2020, and (c) 2000–2020, highlighting areas with statistically significant decreases in red

To better understand how specific land cover transitions have contributed to changes in carbon dynamics, a spatial extraction of carbon sequestration values based on LULC change maps was conducted (see Appendix A: Table A2). Quantitative analysis confirms that LULC changes have significantly influenced carbon storage dynamics in Phang Nga Bay over the past two decades. The region experienced a net reduction in stored carbon of approximately 845,000 Mg C between 2000 and 2010, followed by a smaller increase of 24,400 Mg C from 2010 to 2020, culminating in a cumulative loss of about 821,000 Mg C. These changes reflect spatiotemporal variations in carbon sequestration potential driven by LULC transitions. The most significant contributor to carbon sequestration losses was the extensive conversion of evergreen forests to other land use types, excluding mangrove forests. These transitions accounted for estimated losses of 1,121,000 Mg C during the first decade (2000–2010), 529,000 Mg C during the second decade (2010–2020), and 1,342,000 Mg C across all evergreen forest conversions identified throughout the study period. Additionally, the conversion of mangrove forests resulted in further reductions in carbon sequestration, with estimated losses of 283,000 Mg C in the first decade, 170,000 Mg C in the second, and 155,000 Mg C over the entire timeframe.

The conversion of para rubber plantations into urban areas, oil palm plantations, and bare land resulted in substantial carbon losses of roughly 193,000 Mg C, 264,000 Mg C, and 248,000 Mg C, respectively. Although certain land use transitions, such as the revegetation of bare land, urban areas, and waterbodies, led to localized increases in carbon storage, these gains were insufficient to offset the broader losses associated with deforestation and agricultural expansion. Notably, carbon sequestration gains occurred when low-carbon land use types, including urban areas, oil palm plantations, and degraded lands, were transformed into higher carbon-storing classes such as Para rubber, evergreen forest, or mangrove forest, resulting in net increases in stored carbon. Among all LULC types, evergreen forests exhibited the most consistent and substantial carbon losses, highlighting their vulnerability to land conversion pressures. Despite a reduction in their spatial extent, evergreen forests remained a vital carbon sink, contributing between 14.8% and 26.9% of the region's total carbon storage across the study period. In contrast, mangrove forests, while occupying only 19.3% to 20.0% of the total area, consistently contained the largest carbon stocks, accounting for 50.7% to 55.5% of the regional total. These findings underscore the pivotal role of both evergreen and mangrove forests in sustaining regional carbon reserves and emphasize their ecological significance for climate change mitigation and coastal ecosystem conservation [65] and [66].

Collectively, these results highlight the environmental costs associated with continued agricultural expansion and unregulated land conversion. They also underscore the urgent need for evidence-based and sustainable land management strategies. Preserving high-carbon ecosystems, particularly mangroves and evergreen forests, should be prioritized within land use planning frameworks to maintain a balance between economic development and the provision of ecosystem services, especially long-term carbon sequestration [67] and [68].

3.3 Impacts of Land Use Transitions on Carbon Storage along Elevation

The influence of LULC change on carbon storage along elevation gradients was examined by analyzing total carbon storage across five elevation categories (Figure 7). Results revealed a clear spatial variation in carbon storage, with the highest values observed at the lowest elevation level (<100 meters), reaching up to 13,000,000 Mg C. This is largely attributed to the dominance of mangrove forests in these low-lying coastal zones, which contain both the largest carbon pools (Table 1) and the second-largest spatial extent. In contrast, carbon storage across higher elevation levels (100–400 meters and >400 meters) was considerably lower, with values not exceeding 2,000,000 Mg C. These findings suggest that elevation plays a critical role in shaping the spatial distribution of carbon storage in the study area.

Trend analysis (Figure 7) indicates that carbon storage declined across all elevation levels between 2000 and 2020. Although a modest increase was recorded at the lowest elevation between 2010 and 2020, the overall 20-year trend reflects a net loss in carbon storage. The most substantial declines occurred at mid-elevation ranges (100–400 meters), where a pronounced negative trend was observed (R^2 = 0.99). As shown in Figure 8, the percentage change in carbon storage was lowest (approximately 25%) between 100 and 200 meters but increased at higher elevations, particularly above 300 meters. Notably, the rate of carbon loss during 2010–2020 was lower than during 2000–2010, especially at elevations above 300 meters. This pattern may be attributed to a decline in land conversion intensity during the latter period, particularly the reduced expansion of oil palm and para rubber plantations from evergreen forest, as reflected in Tables 4 and 5.

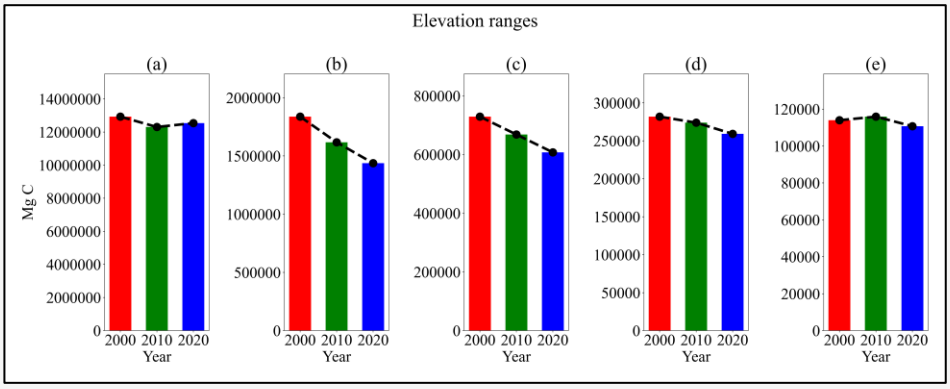

Figure 7: Trends in carbon storage along elevation between 2000 and 2020: (a) lower than 100 m, (b) 100–200 m, (c) 200–300 m, (d) 300–400 m, and (e) higher than 400 m

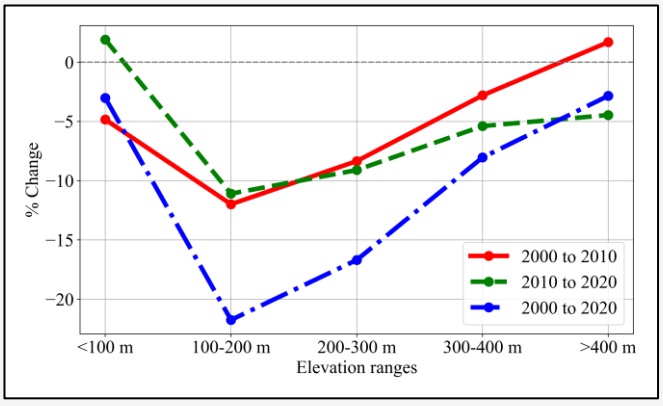

Figure 8: The percentage of carbon storage change along elevation

To better understand the drivers of these trends, carbon storage changes resulting from specific LULC transitions were analyzed across all elevation levels. Figures 9 presents the results for the periods 2000–2010, 2010–2020, and 2000–2020. Between 2000 and 2010 (Figure 9(a)), the most significant contributors to carbon loss below 100 meters were the conversion of evergreen forest to oil palm (approximately 367,000 Mg C), mangrove forest to water (231,000 Mg C), and evergreen forest to para rubber (225,000 Mg C). Although some transitions contributed to localized carbon gains, such as the conversion of bare land to para rubber (198,000 Mg C), oil palm (126,000 Mg C), mangrove forest (110,000 Mg C), and oil palm to mangrove forest (113,000 Mg C), the overall net effect was a reduction in carbon storage. During the 2010–2020 period (Figure 9(b)), similar transition patterns were observed, albeit with reduced intensity. Evergreen forest continued to be converted to oil palm (roughly 190,000 Mg C) and para rubber (61,100 Mg C), but positive transitions such as water to mangrove forest (377,000 Mg C) and water to evergreen forest (106,000 Mg C) contributed to some recovery in carbon stocks. Nevertheless, over the full 2000–2020 period (Figure 9(c)), oil palm expansion remained the dominant driver of carbon loss, especially at elevations up to 200 meters.

At higher elevations (>400 meters), carbon losses were primarily driven by the conversion of evergreen forest to oil palm and para rubber. Although less frequent than in lowland areas, these transitions still contributed meaningfully to upland carbon reductions. Additionally, a few classification anomalies were identified at elevations above 100 meters, where transitions between mangrove and evergreen forest were recorded. Given that mangrove forests are typically restricted to low-lying, coastal zones, these rare cases, such as the two misclassified pixels above 400 meters, are likely attributable to spectral similarities between dense forest canopies or to terrain-related confusion. While the overall impact of such instances on carbon estimates is negligible, the results suggest that classification accuracy in complex forested terrains could be further improved by incorporating ancillary environmental data such as proximity to coastline and tidal inundation zones.

Overall, the decline in carbon storage across all elevation levels reflects a broader trend of forest degradation, primarily driven by the conversion of natural forests to oil palm and Para rubber plantations. While the most pronounced transitions were concentrated in lowland areas, land use change also extended into upland zones. Notably, conversions were detected at elevations exceeding 400 meters, confirming the upward expansion of agricultural activities. This mirrors trends across mountainous mainland Southeast Asia, where rubber plantations have increasingly expanded into non-traditional environments above 300 meters, replacing secondary forests and swidden systems [69]. This spatial trend is consistent with findings from other parts of southern Thailand, including Phang Nga Bay, where oil palm and Para rubber cultivation dominate the agricultural economy [70]. Furthermore, existing literature emphasizes that elevation, population density, and economic incentives significantly influence LULC change [71]. For instance, simulation studies in Indonesia demonstrate that the substantial economic benefits of oil palm for district revenue and employment often outweigh conservation interests, driving rapid forest conversion despite protected status [72]. Government policies have also played a key role in encouraging local communities to expand oil palm cultivation into higher elevation areas. In addition, these policies have facilitated the conversion of carbon-rich peat swamp forests, resulting in significant reductions in carbon stocks and disruptions to ecosystem functions [73].

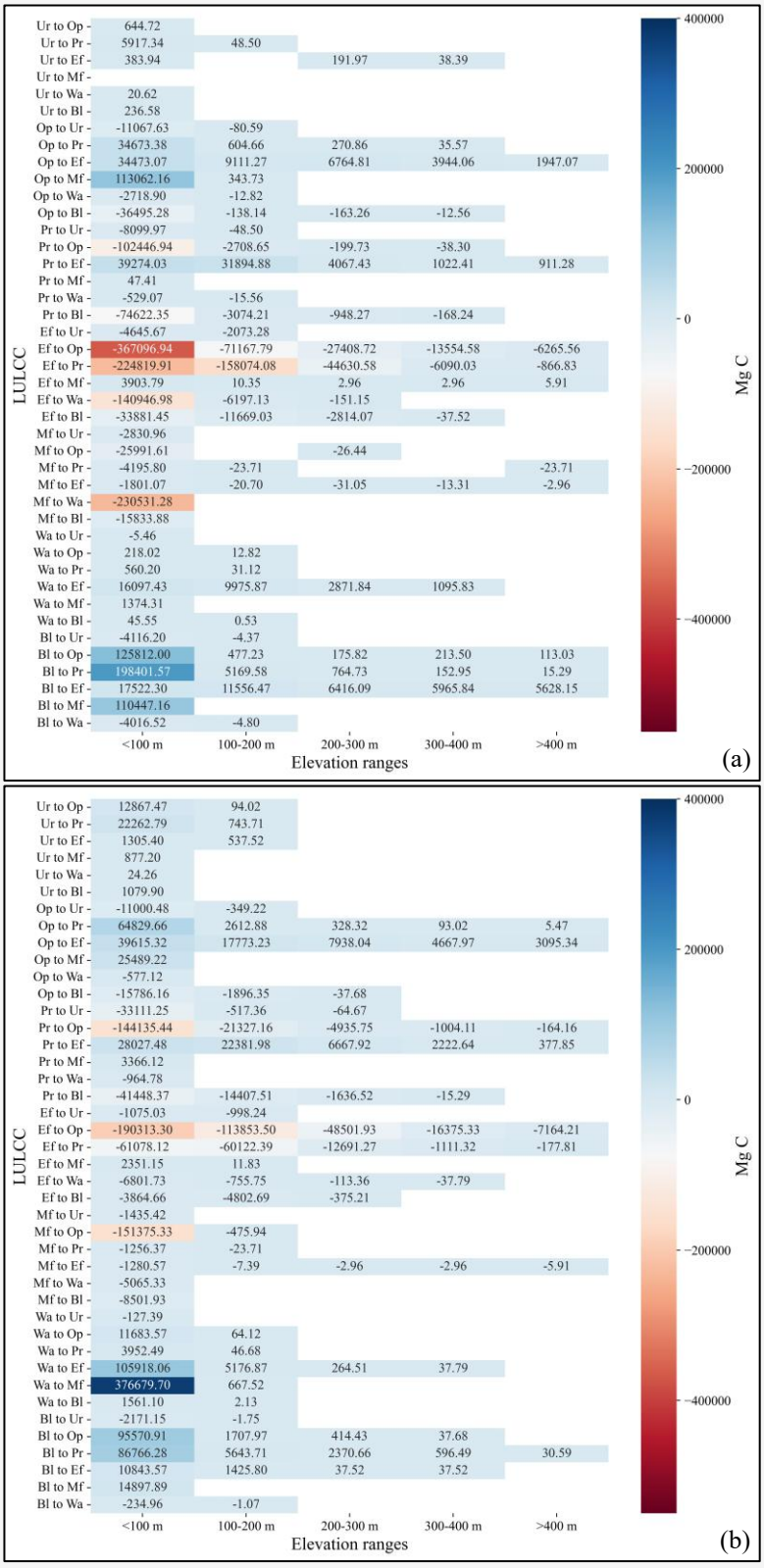

Figure 9: Changes in carbon storage (Mg C) resulting from LULC transitions along elevation: (a) 2000–2010, (b) 2010–2020, and (c) 2000–2020 (continue next page)

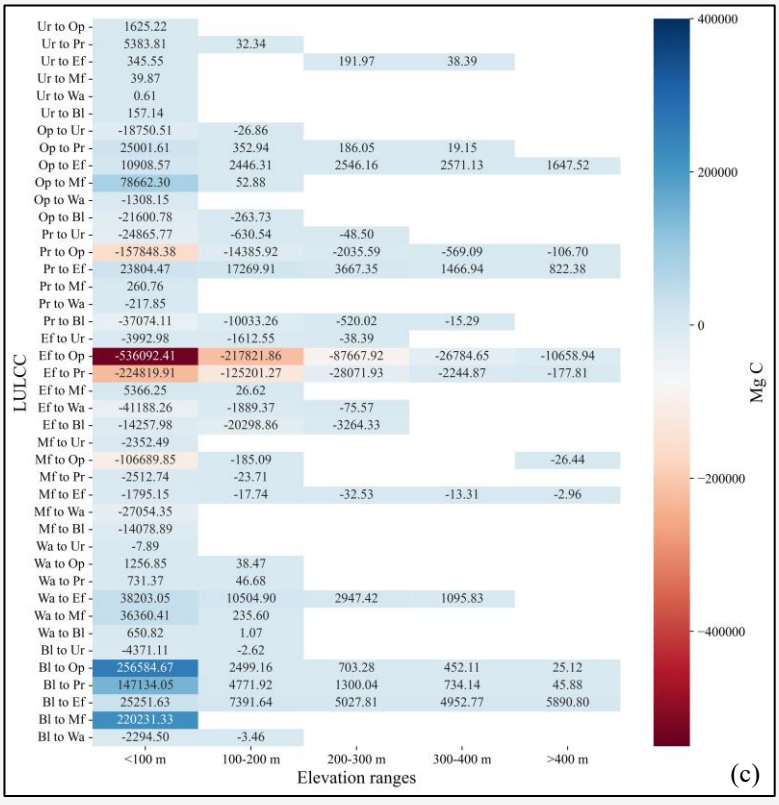

Figure 9: Changes in carbon storage (Mg C) resulting from LULC transitions along elevation: (a) 2000–2010, (b) 2010–2020, and (c) 2000–2020 (continue from previous page)

Similarly, the conversion of forests to rubber monocultures in the region has been linked to accelerated soil erosion, reduced water availability, and declines in soil organic carbon stocks [69]. These findings highlight the urgent need for integrated land management strategies that consider both ecological vulnerability and socio-economic drivers. The protection of forested landscapes, particularly in upland and peatland regions, is essential for mitigating carbon emissions and ensuring the long-term resilience of regional ecosystems.

4. Conclusions

This study provides a comprehensive assessment of LULC change and its implications for carbon storage and sequestration in Phang Nga Bay, southern Thailand, over the period 2000–2020. By integrating the RF classification algorithm in GEE with the InVEST carbon storage and sequestration model, the study achieved high classification accuracy and effectively quantified spatiotemporal carbon dynamics across different land cover types and elevation gradients. The findings reveal substantial LULC change, primarily driven by the rapid expansion of oil palm plantations, which replaced extensive areas of para rubber plantations, evergreen forests, and bare land. This transition, influenced by government incentives and global biodiesel demand, contributed to a substantial net loss in regional carbon storage. The most significant reductions were associated with forest conversion, with the largest carbon sequestration losses occurring during the first decade due to the clearing of evergreen forests. Continued conversion of evergreen forests further contributed to sequestration losses throughout the study period. In contrast to this declining trend, mangrove forests remained a stable and critical component of the region's carbon balance. Although covering a relatively small proportion of the area, they consistently contributed the majority of total carbon storage, emphasizing their role as long-term carbon sinks. Moreover, spatial analysis revealed that while some mangrove forests were lost, mainly to water bodies and oil palm, these losses were offset by gains in other areas, resulting in a net positive sequestration balance.

A critical spatial pattern emerged regarding elevation: carbon storage declined across all zones, with the sharpest reductions occurring in mid-elevation ranges. This pattern reflects upward agricultural encroachment into forested areas. Although partial carbon recovery occurred in

lowland zones after 2010, these gains were not sufficient to reverse the overall declining trend. Importantly, the combined use of GEE-based Random Forest classification and the InVEST carbon model demonstrates the value of a scalable, reproducible, and computationally efficient methodology for assessing ecosystem carbon in complex coastal terrains. This integrated framework reduces reliance on resource-intensive field surveys while providing spatially explicit, elevation-aware insights into carbon dynamics. The methodological approach presented here offers a transferable model for other tropical coastal regions experiencing rapid land use transformation. These findings underscore the urgent need for elevation-sensitive and spatially explicit land management strategies that balance agricultural development with ecosystem conservation. Protecting and restoring high-carbon ecosystems, especially evergreen and mangrove forests, is critical for sustaining carbon sequestration and enhancing climate resilience. Future policies should encourage sustainable land use practices while supporting local livelihoods, and further research is recommended to explore alternative approaches that integrate environmental and socio-economic goals.

5. Limitations and Future work

Although the present classification framework, based on spectral reflectance, key vegetation and water indices, and SRTM elevation, achieved high accuracy, additional feature types may further enhance class separability in future studies. Textural descriptors such as Gray-Level Co-occurrence Matrix (GLCM) metrics and topographic derivatives such as Terrain Ruggedness Index (TRI) and Topographic Wetness Index (TWI) could improve the discrimination of spectrally similar plantation types, including oil palm and rubber. Moreover, fractional cover approaches, particularly linear spectral-mixture modeling, may offer a more nuanced representation of transitional coastal environments such as mudflats and aquaculture ponds, where mixed spectral signals are common. Incorporating these techniques in future work, together with spatial-autocorrelation assessments such as Moran's I and analyses of clustered change patterns, could refine land-cover mapping and strengthen carbon assessments in heterogeneous or ecotonal landscapes. Regarding the monitoring of smaller or fragmented zones, this study recommends integrating high-resolution imagery (e.g., Sentinel-2 or UAVs) to investigate fine-scale land-use dynamics, offering detailed insights that complement the regional-scale patterns assessed in this study. Future research integrating these advanced datasets and methodological enhancements would support more precise detection of landscape changes and improve the robustness of carbon storage estimations in complex coastal ecosystems.

Acknowledgements

The authors express their gratitude to Google Earth Engine for providing imagery data and the platform for LULC classification. Special thanks are extended to the Natural Capital Project at Stanford University for developing the InVEST model, which was instrumental in facilitating the carbon modeling required for this research.

References

[1] Marlianingrum, P. R., Kusumastanto, T., Adrianto, L. and Fahrudin, A., (2021). Valuing Habitat Quality for Managing Mangrove Ecosystem Services in Coastal Tangerang District, Indonesia. *Marine Policy*, Vol. 133(60). https://doi.org/10.1016/j.marpol.2021.104747.

[2] Kamlang-Ek, A., (2010). *Use Value of Mangrove Forest in Southern Region of Thailand.* Proceedings of 48th Kasetsart University Annual Conference: Economics and Business Administration, Bangkok, Thailand, February 3-5, 2010.

[3] Zhu, L., Song, R., Sun, S., Li, Y. and Hu, K., (2022). Land Use/Land Cover Change and Its Impact on Ecosystem Carbon Storage in Coastal Areas of China from 1980 to 2050. *Ecological Indicators*, Vol. 142. https://doi.org/10.1016/j.ecolind.2022.109178.

[4] Borges, A. V., Delille, B. and Frankignoulle, M., (2005). Budgeting Sinks and Sources of CO2 in the Coastal Ocean: Diversity of Ecosystem Counts. *Geophysical Research Letters*, Vol. 32(14). https://doi.org/10.1029/2005GL023053.

[5] Yusup, Y., Swesi, A. E., Sigid, M. F., Almdhun, H. M. and Jamshidi, E. J., (2023). The Relationship between Carbon Dioxide Flux and Environmental Parameters at a Tropical Coastal Sea on Different Timescales. *Marine Pollution Bulletin*, Vol. 193. https://doi.org/10.1016/j.marpolbul.2023.115106.

[6] Beaumont, N. J., Jones, L., Garbutt, A., Hansom, J. D. and Toberman, M., (2014). The Value of Carbon Sequestration and Storage in Coastal Habitats. *Estuarine, Coastal and Shelf Science*, Vol. 137. https://doi.org/10.1016/j.ecss.2013.11.022.

[7] Sommer, R. and Bossio, D., (2014). Dynamics and Climate Change Mitigation Potential of Soil Organic Carbon Sequestration. *Journal of Environmental Management*, Vol. 144. https://doi.org/10.1016/j.jenvman.2014.05.017.

[8] Buotte, P. C., Law, B. E., Ripple, W. J. and Berner, L. T., (2020). Carbon Sequestration and Biodiversity Co-Benefits of Preserving Forests in the Western United States. *Ecological Applications*, Vol. 30(2). https://doi.org/10.1002/eap.2039.

[9] Hopkinson, C. S., Cai, W. J. and Hu, X., (2012). Carbon Sequestration in Wetland Dominated Coastal Systems-a Global Sink of Rapidly Diminishing Magnitude. *Current Opinion in Environmental Sustainability*, Vol. 4. https://doi.org/10.1016/j.cosust.2012.03.005.

[10] Hao, S., Zhu, F. and Cui, Y., (2021). Land Use and Land Cover Change Detection and Spatial Distribution on the Tibetan Plateau. *Scientific Reports*, Vol. 11(1). https://doi.org/10.1038/s41598-021-87215-w.

[11] Li, Z., Liu, W. Z. and Zheng, F. L., (2013). The Land Use Changes and Its Relationship with Topographic Factors in the Jing River Catchment on the Loess Plateau of China. *SpringerPlus*, Vol. 2(1). https://doi.org/10.1186/2193-1801-2-S1-S3.

[12] Aye, W. N., Tong, X., Li, J. and Tun, A. W., (2023). Assessing the Carbon Storage Potential of a Young Mangrove Plantation in Myanmar. *Forests*, Vol. 14(4). https://doi.org/10.3390/f14040824.

[13] Harishma, K. M., Sandeep, S. and Sreekumar, V. B., (2020). Biomass and Carbon Stocks in Mangrove Ecosystems of Kerala, Southwest Coast of India. *Ecological Processes*, Vol. 9(1). https://doi.org/10.1186/s13717-020-00227-8.

[14] Khasanah, N., van Noordwijk, M. and Ningsih, H., (2015). Aboveground Carbon Stocks in Oil Palm Plantations and the Threshold for Carbon-Neutral Vegetation Conversion on Mineral Soils. *Cogent Environmental Science*, Vol. 1(1). https://doi.org/10.1080/23311843.2015.1119964.

[15] Meng, Y., Bai, J., Gou, R., Cui, X., Feng, J., Dai, Z., Diao, X., Zhu,X. and Lin, G., (2021). Relationships between Above- and Below-Ground Carbon Stocks in Mangrove Forests Facilitate Better Estimation of Total Mangrove Blue Carbon. *Carbon Balance and Management*, Vol. 16(8). https://doi.org/10.1186/s13021-021-00172-9.

[16] He, Y., Jiangming, Zhang, C. and Yang, H., (2023). Spatio-Temporal Evolution and Prediction of Carbon Storage in Kunming Based on PLUS and InVEST models. *Remote Sensing*, Vol. 15(5). https://doi.org/10.3390/rs15051445.

[17] Liu, K., Zhang, C., Zhang, H., Xu, H. and Xia, W., (2023). Spatiotemporal Variation and Dynamic Simulation of Ecosystem Carbon Storage in the Loess Plateau Based on PLUS and InVEST Models. *Land*, Vol. 12(5). https://doi.org/10.3390/land12051065.

[18] Piyathilake, I. D. U. H., Udayakumara, E. P. N., Ranaweera, L. V. and Gunatilake, S. K., (2022). Modeling Predictive Assessment of Carbon Storage Using InVEST Model in Uva Province, Sri Lanka. *Modeling Earth Systems and Environment*, Vol. 8. https://doi.org/10.1007/s40808-021-01207-3.

[19] Adelisardou, F., Zhao, W., Chow, R., Mederly, P., Minkina, T. and Schou, J. S., (2022). Spatiotemporal Change Detection of Carbon Storage and Sequestration in an Arid Ecosystem by Integrating Google Earth Engine and InVEST (The Jiroft plain, Iran). *International Journal of Environmental Science and Technology*, Vol. 19. https://doi.org/10.1007/s13762-021-03676-6.

[20] Sadat, M., Zoghi, M. and Malekmohammadi, B., (2020). Spatiotemporal Modeling of Urban Land Cover Changes and Carbon Storage Ecosystem Services: Case Study in Qaem Shahr County, Iran. *Environment, Development and Sustainability*, Vol. 22. https://doi.org/10.1007/s10668-019-00565-4.

[21] Imran, M. and Din, N., (2021). Geospatially Mapping Carbon Stock for Mountainous Forest Classes Using InVEST Model and Sentinel-2 Data: a Case of Bagrote Valley in the Karakoram Range. *Arabian Journal of Geosciences*, Vol. 14(9). https://doi.org/10.1007/s12517-021-07023-4.

[22] Huang, C., Zhang, C. and Li, H., (2022). Assessment of the Impact of Rubber Plantation Expansion on Regional Carbon Storage Based on Time Series Remote Sensing and the InVEST Model. *Remote Sensing*, Vol. 14(24). https://doi.org/10.3390/rs14246234.

[23] Aitali, R., Snoussi, M., Kolker, A. S., Oujidi, B. and Mhammdi, N., (2022). Effects of Land Use/Land Cover Changes on Carbon Storage in North African Coastal Wetlands. *Journal of Marine Science and Engineering*, Vol. 10(3). https://doi.org/10.3390/jmse10030364.

[24] Kacem, H. A., Bouroubi, Y., Khomalli, Y., Elyaagoubi, S., Maanan, M., Rhinane, H. and Maanan, M., (2022). The Economic Benefit of Coastal Blue Carbon Stocks in a Moroccan Lagoon Ecosystem: a Case Study at Moulay Bousselham Lagoon. *Wetlands*, Vol. 42. https://doi.org/10.1007/s13157-022-01533-x.

[25] Rosa, L. N., Duarte de Paula Costa, M. and de Freitas, D. M., (2022). Modelling Spatial-Temporal Changes in Carbon Sequestration by Mangroves in an Urban Coastal Landscape. *Estuarine, Coastal and Shelf Science*, Vol. 276. https://doi.org/10.1016/j.ecss.2022.108031.

[26] Department of Marine and Coastal Resources, Ministry of Natural Resource and Environment. (2023). *Phang Nga Bay Ecosystem* (in Thai). [Online]. Available: https://km.dmcr.go.th/c_218/s_499/d_19709. [Accessed: Apr. 5, 2024]

[27] Office of Natural Resources and Environmental Policy and Planning. (2020). *National Report on the Implementation of Convention on Wetlands Thailand* (in Thai). [Online]. Available: https://chm-thai.onep.go.th/wp-content/uploads/2023/03/48-รายงานแห่งชาติเรื่องพื้นที่ชุ่มน้ำของประเทศไทย.pdf. [Accessed: Apr. 8, 2024]

[28] Prince of Songkla University. (2005). *Land Resource Status and Land Use Planning in the Phang Nga Bay Area* (in Thai). Bangkok: Integrated Promotion Technology.

[29] Breiman, L., (2001). Random Forests. *Machine Learning*, Vol. 45. http://dx.doi.org/10.1023/A:1010933404324.

[30] Belgiu, M. and Drăgu, L., (2016). Random Forest in Remote Sensing: A Review of Applications and Future Directions. *ISPRS Journal of Photogrammetry and Remote Sensing*, Vol. 114. https://doi.org/10.1016/j.isprsjprs.2016.01.011.

[31] Gislason, P. O., Benediktsson, J. A. and Sveinsson, J. R., (2006). Random Forests for Land Cover Classification. *Pattern Recognition Letters*, Vol. 27(4). https://doi.org/10.1016/j.patrec.2005.08.011.

[32] Congalton, R. G., (1991). A review of Assessing the Accuracy of Classifications of Remotely Sensed Data. *Remote Sensing of Environment*, Vol. 37(1). https://doi.org/10.1016/0034-4257(91)90048-B.

[33] Foody, G. M., (2020). Explaining the Unsuitability of the Kappa Coefficient in the Assessment and Comparison of the Accuracy of Thematic Maps Obtained by Image Classification. *Remote Sensing of Environment*, Vol. 239. https://doi.org/10.1016/j.rse.2019.111630.

[34] Jensen, J. R., (2015). *Introductory Digital Image Processing: A Remote Sensing Perspective (4 th).* Illinois: Pearson Education.

[35] Arunyawat, S. and Shrestha, R. P., (2016). Assessing Land Use Change and Its Impact on Ecosystem Services in Northern Thailand. *Sustainability*, Vol. 8(8). https://doi.org/10.3390/su8080768.

[36] Avtar, R., Rinamalo, A. V., Umarhadi, D. A., Gupta, A., Khedher, K. M., Yunus, A. P., Singh, B.P., Kumar, P., Sahu, N. and Sakti, A. D., (2022). Land Use Change and Prediction for Valuating Carbon Sequestration in Viti Levu Island, Fiji. *Land*, Vol. 11(8). https://doi.org/10.3390/land11081274.

[37] Chang, X., Xing, Y., Wang, J., Yang, H. and Gong, W., (2022). Effects of Land Use and Cover Change (LUCC) on Terrestrial Carbon Stocks in China between 2000 and 2018. *Resources, Conservation and Recycling*, Vol. 182. https://doi.org/10.1016/j.resconrec.2022.106333.

[38] Garrastazú, M. C., Mendonça, S. D., Horokoski, T. T., Cardoso, D. J., Rosot, M. A. D., Nimmo, E. R. and Lacerda, A. E. B., (2015). Carbon Sequestration and Riparian Zones: Assessing the Impacts of Changing Regulatory Practices in Southern Brazil. *Land Use Policy*, Vol. 42. https://doi.org/10.1016/j.landusepol.2014.08.003.

[39] Ghafoor, G. Z., Sharif, F., Shahid, M. G., Shahzad, L., Rasheed, R. and Khan, A. U. H., (2022). Assessing the Impact of Land Use Land Cover Change on Regulatory Ecosystem Services of Subtropical Scrub Forest, Soan Valley Pakistan. *Scientific Reports*, Vol. 12. https://doi.org/https://doi.org/10.1038/s41598-022-14333-4.

[40] Gupta, S., Nainwal, A., Anand, S. and Singh, S., (2017). Valuation of Carbon Sequestration in Bidhalna Microwatershed, Uttarakhand, India Using Invest Model. *International Journal of Advancement in Earth and Environmental Sciences*, Vol. 5(1). https://doi.org/10.13140/RG.2.2.29675.90404.

[41] Sharp, R., Douglass, J., Wolny, S., Arkema, K., Bernhardt, J., Bierbower, W., Chaumont, N., Denu, D., Fisher, D., Glowinski, K., Griffin, R., Guannel, G., Guerry, A., Johnson, J., Hamel, P., Kennedy, C., Kim, C.K., Lacayo, M., Lonsdorf, E., Mandle, L., Rogers, L., Silver, J., Toft, J., Verutes, G., Vogl, A. L., Wood, S. and Wyatt, K., 2020, InVEST 3.8.9 User's Guide. *The Natural Capital Project, Stanford University, University of Minnesota, The Nature Conservancy, and World Wildlife Fund*.

[42] He, C., Zhang, D., Huang, Q. and Zhao, Y., (2016). Assessing the Potential Impacts of Urban Expansion on Regional Carbon Storage by Linking The LUSD-Urban and InVEST Models. *Environmental Modelling and Software*, Vol. 75. https://doi.org/10.1016/j.envsoft.2015.09.015.

[43] Islam, I., Cui, S., Hoque, M. Z., Abdullah, H. M., Tonny, K. F., Ahmed, M., Ferdush, J., Xu, L. and Ding, S., (2022). Dynamics of Tree outside Forest Land Cover Development and Ecosystem Carbon Storage Change in Eastern Coastal Zone, Bangladesh. *Land*, Vol. 11(1). https://doi.org/10.3390/land11010076.

[44] Zheng, H. and Zheng, H., (2023). Assessment And Prediction of Carbon Storage Based on Land Use/Land Cover Dynamics in the Coastal Area of Shandong Province. *Ecological Indicators Journal*, Vol. 153. https://doi.org/10.1016/j.ecolind.2023.110474.

[45] Aalde, H., Gonzalez, P., Gytarsky, M., Krug, T., Kurz, W. A., Lasco, R. D., Martino, D. L., McConkey, B. G., Ogle, S., Paustian, K., Raison, J., Ravindranath, N. H., Schoene, D., Smith, P., Somogyi, Z., van Amstel, A. and Verchot, L., (2006). Generic Methodologies Applicable to Multiple Land-Use Categories. *2006 IPCC Guidelines for National Greenhouse Gas Inventories.* Hayama: Institute for Global Environmental Strategies.

[46] Xiang, H., Jia, M., Wang, Z., Li, L., Mao, D., Zhang, D., Cui, G. and Zhu, W., (2018). Impacts of Land Cover Changes on Ecosystem Carbon Stocks Over the Transboundary Tumen River Basin in Northeast Asia. *Chinese Geographical Science*, Vol. 28(6). https://doi.org/10.1007/s11769-018-1006-y.

[47] Afentina, Patimaleh, I. B. and Kurniadi., (2022). Above Ground Carbon Stock across Different Land Use Types in Central Kalimantan Indonesia – First Step Toward Redd Implementation. *Journal of Ecological Engineering*, Vol. 23(8). https://doi.org/10.12911/22998993/151072.

[48] Khalid, H., Zin, Z. and Anderson, J. M., (1999). Quantification of Oil Palm Biomass and Nutrient Value in a Mature Plantation. II. Below-Ground Biomass. *Journal of Oil Palm Research*, Vol. 11(2), 63–71.

[49] Handayani, I. P., Widiastuti, H., Coyne, M. S. and Widawati, S., (2020). Soil Organic Carbon Fractions in Oil Palm Management Systems. *IOP Conference Series: Earth and Environmental Science*, Vol. 583. https://doi.org/10.1088/1755-1315/583/1/012006.

[50] Singh, S. L., Sahoo, U. K., Kenye, A. and Gogoi, A., (2018). Assessment of Growth, Carbon Stock and Sequestration Potential of Oil Palm Plantations in Mizoram, Northeast India. *Journal of Environmental Protection*, Vol. 9(9). https://doi.org/10.4236/jep.2018.99057.

[51] Jia, P., Huang, W., Zhang, Z., Cheng, J. and Xiao, Y., (2022). The Carbon Sink of Mangrove Ecological Restoration between 1988–2020 in Qinglan Bay, Hainan Island, China. *Forests*, Vol. 13(10). https://doi.org/10.3390/f13101547.

[52] Gong, W., Duan, X., Mao, M., Hu, J., Sun, Y., Wu, G., Zhang, Y., Xie, Y., Qiu, X., Rao, X., Liu, T. and Liu, T., (2022). Assessing the Impact of Land Use and Changes in Land Cover Related to Carbon Storage by Linking Trajectory Analysis and InVEST Models in the Nandu River Basin on Hainan Island in China. *Frontiers in Environmental Science*, Vol. 10. https://doi.org/10.3389/fenvs.2022.1038752.

[53] Li, J., Yan, D., Yao, X., Liu, Y., Xie, S., Sheng, Y. and Luan, Z., (2022). Dynamics of Carbon Storage in Saltmarshes Across China's Eastern Coastal Wetlands From 1987 to 2020. *Frontiers in Marine Science*, Vol. 9. https://doi.org/10.3389/fmars.2022.915727.

[54] Zhao, Y., An, R., Xiong, N., Ou, D. and Jiang, C., (2021). Spatio-Temporal Land-Use/Land-Cover Change Dynamics in Coastal Plains in Hangzhou Bay Area, China from 2009 to 2020 Using Google Earth Engine. *Land*, Vol. 10(11). https://doi.org/10.3390/land10111149.

[55] Zeng, J., Ai, B., Jian, Z., Ye, M., Zhao, J. and Sun, S., (2023). Analysis of Mangrove Dynamics and Its Protection Effect in the Guangdong-Hong Kong-Macao Coastal Area Based on the Google Earth Engine Platform. *Frontiers in Marine Science*, Vol. 10. https://doi.org/10.3389/fmars.2023.1170587.

[56] Kumar, L. and Mutanga, O., (2018). Google Earth Engine Applications Since Inception: Usage, Trends, and Potential. *Remote Sensing*, Vol. 10(10). https://doi.org/10.3390/rs10101509.

[57] Prasetthanon, S., (2004). *Strategic of Oil Plam Industry Year 2004-2029 (12 Nov. 2004)* (in Thai). Office of Agricultural Economics.

[58] Office of the National Economic and Social Development Council. (2009). *Annual Report 2009 (1st printing)* (in Thai). Bangkok: Office of Development Evaluation and Publication.

[59] Mekhilef, S., Siga, S. and Saidur, R., (2011). A Review on Palm Oil Biodiesel as a Source of Renewable Fuel. *Renewable and Sustainable Energy Reviews*, Vol. 15(4). https://doi.org/10.1016/j.rser.2010.12.012.

[60] Austin, K. G., Mosnier, A., Pirker, J., McCallum, I., Fritz, S. and Kasibhatla, P. S., (2017). Shifting Patterns of Oil Palm Driven Deforestation in Indonesia and Implications for Zero-Deforestation Commitments. *Land Use Policy*, Vol. 69. https://doi.org/10.1016/j.landusepol.2017.08.036.

[61] Ziegler, A. D., Phelps, J., Yuen, J. Q., Webb, E. L., Lawrence, D., Fox, J. M., Bruun, T. B., Leisz, S. J., Ryan, C. M., Dressler, W., Mertz, O., Pascual, U., Padoch, C. and Koh, L. P., (2012). Carbon Outcomes of Major Land-Cover Transitions in SE Asia: Great Uncertainties and REDD+ Policy Implications. *Global Change Biology*, Vol. 18. https://doi.org/10.1111/j.1365-2486.2012.02747.x.

[62] Wicke, B., Sikkema, R., Dornburg, V. and Faaij, A., (2011). Exploring Land Use Changes and the Role of Palm Oil Production in Indonesia and Malaysia. *Land Use Policy*, Vol. 28(1). https://doi.org/10.1016/j.landusepol.2010.06.001.

[63] Hansen, M. C., Potapov, P. V., Moore, R., Hancher, M., Turubanova, S. A., Tyukavina, A., Thau, D., Stehman, S. V., Goetz, S. J., Loveland, T. R., Kommareddy, A., Egorov, A., Chini, L., Justice, C. O. and Townshend, J. R. G., (2013). High-Resolution Global Maps of 21st-Century Forest Cover Change. *Science*, Vol. 342(6160). https://doi.org/10.1126/science.1244693.

[64] Margono, B., Potapov, P., Turubanova, S., Stolle, F. and Hansen, M., (2014). Primary Forest Cover Loss in Indonesia over 2000–2012. *Nature Climate Change*, Vol. 4. https://doi.org/doi:10.1038/nclimate2277.

[65] Alongi, D. M., (2014). Carbon Cycling and Storage in Mangrove Forests. *Annual Review of Marine Science*, Vol. 6. https://doi.org/10.1146/annurev-marine-010213-135020.

[66] Richards, D. R. and Friess, D. A., (2016). Rates and Drivers of Mangrove Deforestation in Southeast Asia, 2000–2012. *Proceedings of the National Academy of Sciences*, Vol. 113(2). https://doi.org/10.1073/pnas.1510272113.

[67] Goldstein, J. H., Caldarone, G., Duarte, T. K., Ennaanay, D., Hannahs, N., Mendoza, G., Polasky, S., Wolny, S. and Daily, G. C., (2012). Integrating Ecosystem-Service Tradeoffs into Land-Use Decisions. *Proceedings of the National Academy of Sciences of the United States of America*, Vol. 109(19). https://doi.org/10.1073/pnas.1201040109.

[68] Warren-Thomas, E., Dolman, P. M. and Edwards, D. P., (2015). Increasing Demand for Natural Rubber Necessitates a Robust Sustainability Initiative to Mitigate Impacts on Tropical Biodiversity. *Conservation Letters*, Vol. 8(4). https://doi.org/10.1111/conl.12170.

[69] Fox, J., Castella, J. C., Ziegler, A. D. and Westley, S. B., (2014). *Rubber Plantations Expand in Mountainous Southeast Asia: What Are the Consequences for the Environment?*. East-West Center: Honolulu, HI, USA, 2014; No. 114.

[70] Unjan, R., Nissapa, A. and Chiarawipa, R., (2017). Climatic Considerations which Support the Choice between Natural Rubber and Oil Palm in Nakhon Si Thammarat, Southern Thailand. *Kasetsart Journal of Social Sciences*, Vol. 38(3). https://doi.org/10.1016/j.kjss.2016.07.006.

[71] Wang, Y., Hu, Y., Niu, X., Yan, H. and Zhen, L., (2022). Land Use/Cover Change and Its Driving Mechanism in Thailand from 2000 to 2020. *Land*, Vol. 11(12). https://doi.org/10.3390/land11122253.

[72] Sandker, M., Suwarno, A. and Campbell, B. M., (2007). Will Forests Remain in the Face of Oil Palm Expansion? Simulating Change in Malinau, Indonesia. *Ecology and Society*, Vol. 12(2). https://doi.org/10.5751/ES-02292-120237.

[73] Srisunthon, P. and Chawchai, S., (2020). Land-Use Changes and the Effects of Oil Palm Expansion on a Peatland in Southern Thailand. *Frontiers in Earth Science*, Vol. 8. https://doi.org/10.3389/feart.2020.559868.

[74] Rouse, J. W., Jr., R. H. H., Schell, J. A. and Deering, D. W., (1974). Monitoring Vegetation Systems in the Great Plains with Erts. *Third Earth Resources Technology Satellite-1 Symposium Volume I: Technical Presentations Section A*. Washington D.C.: National Aeronautics and Space Administration, 309-317.

[75] Xu, H., (2006). Modification of Normalised Difference Water Index (NDWI) to Enhance Open Water Features in Remotely Sensed Imagery. *International Journal of Remote Sensing*, Vol. 27(14). https://doi.org/10.1080/01431160600589179.

[76] Zha, Y., Gao, J. and Ni, S., (2003). Use of Normalized Difference Built-Up Index in Automatically Mapping Urban Areas from TM Imagery. *International Journal of Remote Sensing,* Vol. 24(3). https://doi.org/10.1080/01431160304987.

[77] Yue, J., Tian, J., Tian, Q., Xu, K. and Xu, N. (2019). Development of Soil Moisture Indices from Differences in Water Absorption between Shortwave-Infrared Bands. *ISPRS Journal of Photogrammetry and Remote Sensing*, Vol. 154. https://doi.org/10.1016/j.isprsjprs.2019.06.012.

[78] Huete, A. R., (1988). A Soil-Adjusted Vegetation Index (SAVI). *Remote Sensing of Environment*, Vol. 25(3). https://doi.org/10.1016/0034-4257(88)90106-X.

[79] Huete, A., Didan, K., Miura, T., Rodriguez, E. P., Gao, X. and Ferreira, L. G., (2002). Overview of the Radiometric and Biophysical Performance of the MODIS Vegetation Indices. *Remote Sensing of Environment*, Vol. 83. https://doi.org/10.1016/S0034-4257(02)00096-2.

[80] Nguyen, C. T., Chidthaisong, A., Diem, P. K. and Huo, L. Z., (2021). A Modified Bare Soil Index to Identify Bare Land Features During Agricultural Fallow-Period in Southeast Asia Using Landsat 8. *Land*, Vol. 10(3). https://doi.org/10.3390/land10030231.

Appendix

Table A1: Additional spectral Indices for LULC classification

Spectral Index	Equation	Function	References
NDVI	$\frac{NIR-R}{NIR+R}$	This index measures the greenness and health of vegetation by exploiting the contrast between the red and near-infrared reflectance of vegetation.	[74]
MNDWI	$\frac{GREEN-SWIR}{GREEN+SWIR}$	This index can enhance open water features while efficiently suppressing and even removing built-up land noise as well as vegetation and soil noise.	[75]
NDBI	$\frac{SWIR-NIR}{SWIR+NIR}$	This index is tailored to identify urban and built-up areas by leveraging the unique spectral response of these surfaces in the shortwave infrared and near-infrared regions.	[76]
NSDSI3	$\frac{SWIR1-SWIR2}{SWIR1+SWIR2}$	This index effectively targets bare soil by leveraging strong SWIR reflectance compared to water and vegetation.	[77]
SAVI	$1.5 * \frac{NIR-R}{NIR+R+0.5}$	A variation of NDVI, SAVI accounts for the influence of soil background effects, improving vegetation discrimination in areas with sparse vegetation cover.	[78]
EVI	$2.5 * \frac{NIR-R}{NIR+6*R-7.5*B+1}$	Similar to NDVI but with improved sensitivity to high biomass regions, EVI incorporates corrections for atmospheric and soil background effects, providing a more comprehensive assessment of vegetation conditions.	[79]
MBI	$\frac{SWIR1-SWIR2-NIR}{SWIR1+SWIR2+NIR}+0.5$	This index was modified from NSDSI3 to effectively reduce the positive index values associated with vegetation, enhancing the ability to distinguish bare soil areas from vegetated surfaces.	[80]

Table A2: Carbon sequestration (Mg C) associated with LULC transitions in Phang Nga Bay from 2000 to 2020 (Continue next page)

LULC change	2000–2010			2010–2020			2000–2020		
	Area km^2	Mg C		Area km^2	Mg C		Area km^2	Mg C	
Ur-to-Op	0.04	644.72	7,489.66	0.87	12,961.51	39,793.18	0.11	1,638.66	7,831.82
Ur-to-Pr	0.33	5,965.84		1.28	23,006.52		0.30	5,416.15	
Ur-to-Ef	0.01	614.30		0.04	1,842.91		0.01	575.91	
Ur-to-Mf	0.00	0.00		0.02	877.20		0.00	39.87	
Ur-to-Wa	0.03	21.23		0.04	24.26		0.00	0.61	
Ur-to-Bl	0.25	243.57		1.11	1,080.78		0.17	160.63	
Op-to-Ur	0.75	−11,148.23	154,898.04	0.76	−11,349.71	136,815.20	1.26	−18,777.37	82,480.04
Op-to-Pr	11.71	35,592.65		22.33	67,883.02		8.42	25,581.62	
Op-to-Ef	2.03	56,439.98		2.64	73,089.98		0.73	20,119.69	
Op-to-Mf	3.87	113,643.85		0.87	25,489.25		2.68	78,741.60	
Op-to-Wa	0.20	−2,795.85		0.04	−577.13		0.09	−1,320.97	
Op-to-Bl	2.64	−36,834.37		1.27	−17,720.20		1.57	−21,864.52	
Pr-to-Ur	0.45	−8,148.47	−115,684.99	1.88	−33,693.31	−200,721.28	1.42	−25,544.81	−201,075.38
Pr-to-Op	34.67	−105,396.27		56.45	−171,599.49		57.55	−174,961.85	
Pr-to-Ef	3.12	77,170.05		2.42	59,677.94		1.90	47,031.05	
Pr-to-Mf	0.00	47.41		0.13	3,366.13		0.01	260.76	
Pr-to-Wa	0.03	−544.64		0.06	−964.78		0.01	−217.85	
Pr-to-Bl	4.64	−78,813.08		3.38	−57,507.76		2.80	−47,642.68	

Table A2: Carbon sequestration (Mg C) associated with LULC transitions in Phang Nga Bay from 2000 to 2020 (Continue form previous page)

LULC change	2000–2010			2010–2020			2000–2020		
	Area km^2	Mg C		Area km^2	Mg C		Area km^2	Mg C	
Ef-to-Ur	0.16	−6,718.95	−1,121,303.88	0.05	−2,073.28	−528,844.58	0.13	−5,643.92	−1,342,404.28
Ef-to-Op	17.51	−485,518.66		13.59	−376,807.80		31.72	−879,874.61	
Ef-to-Pr	17.59	−434,503.83		5.47	−135,203.31		15.41	−380,515.90	
Ef-to-Mf	2.39	3,930.39		1.44	2,368.88		3.29	5,397.26	
Ef-to-Wa	3.57	−149,978.18		0.19	−8,086.51		1.04	−43,833.38	
Ef-to-Bl	1.16	−48,514.65		0.22	−9,042.57		0.91	−37,933.73	
Mf-to-Ur	0.06	−2,830.96	−282,901.52	0.03	−1,435.42	−170,232.23	0.05	−2,352.49	−155,244.91
Mf-to-Op	0.89	−26,018.04		5.19	−152,459.55		3.65	−107,086.46	
Mf-to-Pr	0.16	−4,243.21		0.05	−1,351.19		0.10	−2,536.45	
Mf-to-Ef	1.14	−1,873.52		0.79	−1,301.26		1.13	−1,861.69	
Mf-to-Wa	5.32	−232,101.91		0.12	−5,143.86		0.63	−27,289.94	
Mf-to-Bl	0.37	−15,833.88		0.20	−8,540.94		0.33	−14,117.89	
Wa-to-Ur	0.01	−5.46	33,093.12	0.20	−134.67	528,789.45	0.02	−10.92	95,765.49
Wa-to-Op	0.02	243.67		0.95	13,543.21		0.10	1,449.22	
Wa-to-Pr	0.03	591.32		0.25	4,310.40		0.05	778.05	
Wa-to-Ef	0.73	30,796.73		2.77	116,460.87		1.33	56,000.92	
Wa-to-Mf	0.03	1,413.58		9.00	392,779.19		0.84	36,831.60	
Wa-to-Bl	0.18	53.28		6.18	1,830.44		2.42	716.62	
Bl-to-Ur	4.26	−4,131.91	479,112.58	2.26	−2,191.23	218,791.70	4.54	−4,405.16	691,741.67
Bl-to-Op	9.09	126,892.08		7.02	97,957.17		18.78	262,097.95	
Bl-to-Pr	12.04	204,611.17		5.63	95,698.41		9.10	154,659.00	
Bl-to-Ef	1.14	47,501.58		0.30	12,644.59		1.20	49,977.97	
Bl-to-Mf	2.58	111,890.14		0.34	14,936.90		5.42	235,012.18	
Bl-to-Wa	25.85	−7,650.48		0.86	−254.15		18.92	−5,600.26	